

Physical Interaction Based Traveling Aid System with Depth Camera and Unevenness Detection Mechanism

Shinya Kajikawa

Department of Mechanical Engineering and Intelligent Systems,
Faculty of Engineering, Tohoku Gakuin University, Tagajo, Japan
Email: kajikawa@mail.tohoku-gakuin.ac.jp

Iori Watanabe

Honda Motor Co., Ltd, Tokyo, Japan
Email: Iori_Watanabe@jp.honda

Hayato Hoshi

TKC Corporation, Utsunomiya, Japan
Email: star9262@gmail.com

Abstract— This paper proposes a physical interaction based travel aid system for the visually impaired. The proposed system connects two steered wheels to the waist of the user through telescopic rods. These wheels are controlled to avoid obstacles or dents in the ground, detected via two sensing modules: a depth camera and a passive fork mechanism for the wheels. When steering control is applied, the resisting force on each wheel from the ground changes and the difference between the forces makes the user unconsciously change walking direction. In this paper, we describe the navigation system and confirm its possibility of safe guidance.

Index Terms—Traveling aid system, Visual impairment, Physical interaction, Steered wheels, Depth camera

I. INTRODUCTION

The World Health Organization (WHO) reported that the number of visually impaired individuals in the world has reached approximately 253 million; of these, 36 million are blind and 217 million have moderate to severe visual impairment [1]. Many types of traveling aid devices have been developed for visually impaired individuals to enable independent living and promote social participation. The primary purpose of these devices is to safely guide the user to their destination; thus, they require two modules: one module for sensing the surrounding environment and the other for presenting the sensed data to the user.

These modules are expected to locate and inform the users of obstacles that would impede independent walking. Ultrasonic sensors are often used in sensor modules owing to their small size and wide coverage area. Haptic feedback systems that alert for low-hanging obstacles (HALO) have been considered as attachable devices to traditional white

canes [2]. In this system, an ultrasonic sensor is utilized to detect an obstacle at the trunk-level height, and a vibration generated by an eccentric motor alert the user to indicate the presence of the obstacle. Augmented white canes (AWCs) have a wider search area from the ground to the head level, with a combination of two ultrasonic sensors and an infrared sensor [3]. The device provides distance information for the detected obstacle via a vibrotactile display. Moreover, an advanced AWC (AAWC) was developed to enlarge the scan area using three ultrasonic sensors and an infrared sensor [4]. The AAWC informs the user of the height and distance of the obstacle through audio and different vibrotactile feedback patterns. A depth camera with a wide sensing area has also been used for navigation [5,6].

Indeed, existing systems focus on improving sensing abilities and obtaining more detailed information regarding the environment. However, the presentation of information to the user is limited based on sound and vibration, and is insufficient for the user to decide a safer walking path. It is difficult to plan a safer route based on the perception of changes in sensory stimulation.

It is necessary to develop a more user-friendly system that removes the perceptual and mental burden and allows unconscious and safe walking. In this paper, “unconscious” is used to describe a state free from perceptual and cognitive processes for induced stimuli. The guide cane with ultrasonic sensor arrays navigates the user by controlling the wheels attached to the distal end [7]. Consequently, the moment generated by the change in the direction of the wheels acts on the hand of the user. The physical interaction allows the user to unconsciously follow a path guided by the system. Navigation utilizing

physical interaction is a good approach; however, interaction with the trunk would be more effective than that with the arm. The reasons for this are as follows:

Generally, humans move in the direction that the trunk is facing; therefore, it is effective to directly control the orientation of the trunk. The human arm has rich degrees of freedom and smaller inertia than the trunk; therefore, it can move flexibly and smoothly to follow guiding forces. However, the user must change the orientation of the trunk based on the somatosensory system to follow guided arm movement. Indirect guidance causes delays and a lack of accuracy.

In this paper, we propose a travel aid system that effectively uses physical interaction based on knowledge of the walking environment, obtained via a depth camera and unevenness detection mechanism. The depth camera detects obstacles and searches for the direction in which the user can avoid collisions.

Conversely, the unevenness detection mechanism provides information on bumps close to the user, which are difficult to detect using a camera. These sensing modules, combined with the two steered wheels, are installed on a frontal plate that is connected to the left and right hips of the user via telescopic rods. When obstacles and bumps were detected, the angle of each steering wheel was controlled to avoid them. As the angle of the steered wheel changes, it causes a difference in the resistance to motion of the two wheels, which generates a rotational moment that alters the direction of travel of the user. This moment is supposed to increase in proportion to the magnitude of the difference in steering angles.

This moment rotates the trunk and allows the user to easily and smoothly change the walking direction and traverse the obstacle region. This study describes the effectiveness of the navigation method using physical interaction and the theoretical and experimental methods of sensing the environment using a depth camera and a dent detection mechanism.

II. SYSTEM STRUCTURE

Fig. 1 illustrates a prototype of the walking guidance system. The system consists of four wheels that rotate passively as the user walks, and a depth camera that detects obstacles ahead and searches for a collision-free zone. In addition to the camera, two out of the four wheels detect dents on either side of the walking route by monitoring the changes in their height position. Besides, the camera and dent detection wheels work complementarily to advance navigation safety.

The other two wheels guide the user to a safer route by updating their steering angles based on the information from the dent detection wheels and the depth camera. These elements are attached to the front plate, which is connected to either sides of the user's waist via telescopic rods.

A. Telescopic Rod

The rod that connects the four wheels and the sensing module to the waist of the user has a telescopic rod-like structure consisting of two pipes with different diameters,

as illustrated in Fig.2. The upper narrow pipe, composed of acrylic resin, has outer and inner diameters of 18.0 mm and 16.0 mm, respectively, while those of the lower wider aluminum pipe have outer and inner diameters of 25.0 mm and 19.0 mm, respectively. The two pipes had equal lengths of 1000 mm, and the overall length became 1560 mm after the narrow pipe is inserted into the wider pipe. When an axial force is exerted, the narrow pipe slides into a wider pipe and the overall length is reduced.

After the force is removed, the narrow pipe returns to its original position owing to the springs attached in an antagonistic arrangement inside or outside the larger pipe. Thus, the relative positions of the two pipes were controlled automatically. This functions well to maintain stable contact between the wheels and the ground during turning movements.

When turning, the turn radius of the inner wheels becomes smaller than that of the outer wheel; thus, the wheel on the outer side tends to float from the ground when shafts of constant length are connected to the waist of the user. The telescopic rod adjusts its length via the resistive frictional force between the wheels and ground, preventing the wheel from floating.

Furthermore, the resistive forces on the right and left rods can be determined based on the stiffness of the two springs and their displacement magnitudes, as measured by a force-sensitive linear potentiometer (FSLP). These forces act on the waist of the user and apply a rotational moment, making the user to face the desired direction. A detailed explanation of this mechanism is provided in a subsequent section.

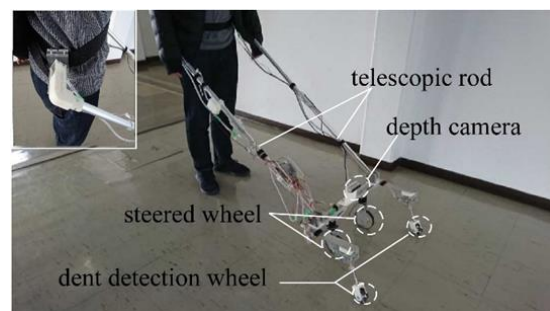


Figure 1. Prototype of the traveling aid system
upper narrow pipe (inner pipe)

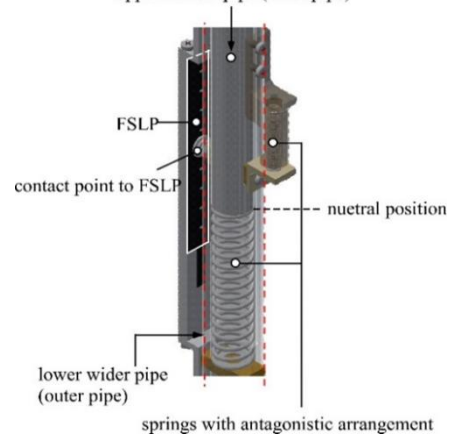


Figure 2. Mechanism of a telescopic rod.

B. Steered Wheel

The steered wheel is illustrated in Fig. 3. The diameter and width are 105.0 mm and 18.0 mm, respectively. The steering angles of the two steered wheels were adjusted via servo motors (RS405CB, Futaba Corporation: Torque (max)=4.7Nm, Speed(max)=0.21s/60deg) to avoid collision with obstacles or to prevent drop-off into a dent. The relationship between the steering angle and the behavior of the user was modeled, and the effectiveness of the steering control was verified experimentally, as presented in a subsequent section.

C. Wheel for Dent Detection

An additional wheel mechanism was implemented to detect dents or steps. This mechanism was fabricated with an omnidirectional wheel (#14145, NEXUS ROBOT: $\phi=60\text{mm}$) and a joystick with a spring actuated self-return force, as depicted in Fig.4. The wheel was attached to the tip of the joystick and is placed in contact with the ground with its stick tilted.

When the wheel falls into a dent, the stick rotates towards its neutral position via a spring. The mechanism detects the dent by measuring the rotational angle using a rotary potentiometer (SV01A103AEA01, MURATA) and generates a control command for the steered wheels to immediately stop the user from walking.

D. Sensing Function of Environment

To act as a safe guide, the system should be able to detect obstacles and determine the safest route through the walking area. For this purpose, we used a depth camera (RealSense D435i, Intel), which offers an active stereo depth with 1280×720 resolution, a 90 fps dense depth stream, and a 2D RGB sensor for color. Furthermore, it is integrated with the cross-platform SDK for Intel@ RealSense™ devices, enabling multiple computing languages and the facile development of an application that satisfies the desired function. The camera was placed 310 mm above the ground and equidistant between the two steered wheels, as illustrated in Fig.1.

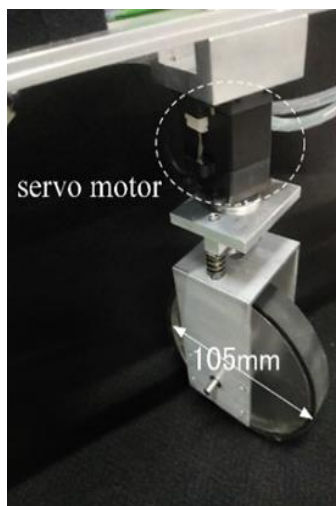


Figure 3. Steered wheel.

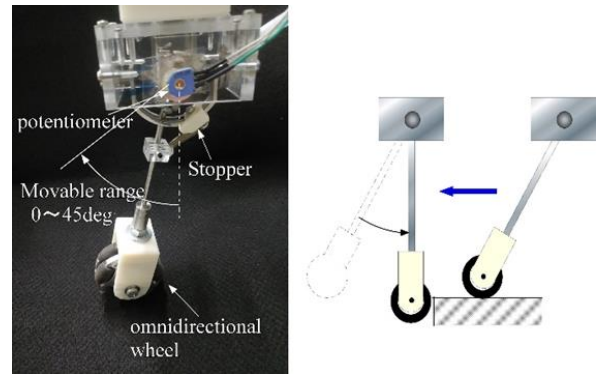


Figure 4. Mechanism of the dent detection wheel.

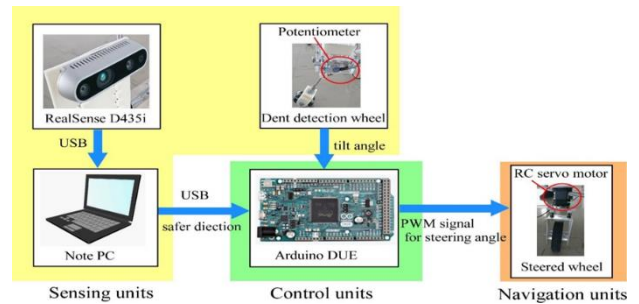


Figure 5. System configuration

E. System Configuration

The system configuration is illustrated in Fig.5. In this system, a note PC and as Arduino DUE were utilized for sensing the environment and user navigation, respectively. Note that the PC obtained image data at 30 fps from RealSense D435i and processed it using the developed software based on both SDK for RealSense™ and the open-source computer vision library OpenCV 4.2.0 C++ in Visual Studio 2019.

Thus, it determines a possible collision-free area and notifies the Arduino DUE via USB interface. Subsequently, the Arduino DUE determines the angle of the steered wheels based on both notifications from the PC and position measurements from the dent detection wheels.

III. GUIDANCE MODEL WITH PHYSICAL INTERACTION

Fig.6 shows a model of the turning movement, projected onto the ground plane. The system was modeled as a rear-drive cart, assuming that the foot of the user was the driving wheel.

In this figure, L , D , and d denote the wheel-base, tread, and distance between two steered wheels, respectively. When the system rotates with a radius R around point O and its turn angle is expressed as θ_d , the angles of the two steered wheels should be set to different values, θ^r and θ^l , as follows:

$$R = \frac{L}{\tan\theta_d} \tag{1}$$

$$\theta^r = \tan^{-1}\left(\frac{L}{R+\frac{d}{2}}\right) \tag{2}$$

$$\theta^l = \tan^{-1}\left(\frac{L}{R-\frac{d}{2}}\right) \tag{3}$$

The driving force, f , generated by the user walking, which is applied equally to the two steered wheels can be divided into $f_{loss}^{r,(l)}$ and $f_{drive}^{r,(l)}$ according to the steered angle, θ^r , and θ^l , respectively:

$$f_{loss}^{r,(l)} = f \sin \theta^{r,(l)} \quad (4)$$

$$f_{drive}^{r,(l)} = f \cos \theta^{r,(l)} \quad (5)$$

$f_{drive}^{r,(l)}$ rotates each wheel forward while $f_{loss}^{r,(l)}$ slips the outer wheel. However, a friction force occurs between the wheel and the ground, $f_{fr}^{r,(l)}$, which prevents slip; thus, the wheels can smoothly move along the steering angles:

$$f_{fr}^{r,(l)} = f_{loss}^{r,(l)} \quad (6)$$

The friction force, $f_{fr}^{r,(l)}$, can be divided into two components, $f_{resist}^{r,(l)}$ and, $f_{trans}^{r,(l)}$ as follows:

$$f_{resist}^{r,(l)} = f_{fr}^{r,(l)} \sin \theta^{r,(l)} \quad (7)$$

$$f_{trans}^{r,(l)} = f_{fr}^{r,(l)} \cos \theta^{r,(l)} \quad (8)$$

Assuming the force, $f_{resist}^{r,(l)}$, is exerted with equal magnitude on the waist of the user via telescopic rods on their right and left sides, these forces act on the user as a rotational moment M about the centroid of their body.

The moment M is defined as:

$$M = \left(\frac{D}{2}\right) (f_{resist}^r - f_{resist}^l) \quad (9)$$

The physical interaction makes the user involuntarily change his/her walking direction.

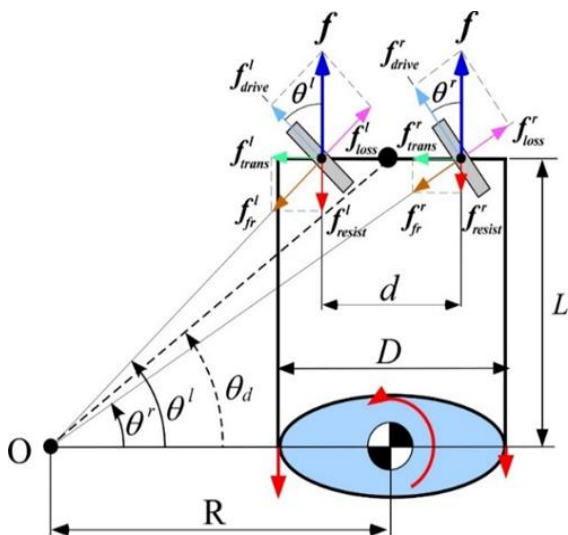


Figure 6. Theoretical model representing the relationship between forces applied to steered wheels and the moment around the craniocaudal axis of the user.

IV. GUIDANCE FOR SAFETY WALKING

The proposed system can detect potentially dangerous situations, such as falling into dents on the ground or colliding with obstacles. In this function, the dent detection mechanism and depth camera are used effectively.

A. Dent Detection

The wheels for dent detection were mounted in front of the left and right-steered wheels. These wheels cover the area close to the user out of the range of the depth camera. More specially, they can detect dents through actual contact with the ground and thus immediately provide reliable information.

As illustrated in Fig. 4, a dent is detected by the change in the tilt angle of the stick of the wheel. When the change exceeds the threshold level, the steering angles of the wheels are controlled to prevent the user from walking. The angles of the right and left wheels, and, were controlled at -45 deg and 45 deg, respectively. The RC servo motor was estimated to take approximately 0.16 s to change the steering angle from 0 deg for a straight walk to -45 deg or 45 deg for an emergency stop. It should be verified if a delay of 0.16 s significantly affects accident prevention.

B. Generation of Safety Map with Depth Camera

Obstacle avoidance is one of the primary issues in the field of mobile robot control; therefore, numerous studies have been conducted to improve obstacle avoidance. They are categorized into two groups; mathematical model-based methods and learning-based methods. The potential filed method [8], dynamic window approach [9], and vector field histogram (VFH) method [10] are well-known mathematical model-based methods. In these methods, a mathematical model is devised to evaluate the likelihood of collision based on the location of the obstacle or kinematic and dynamic constraints of the robot. Based on this model, the robots can generate a suitable path to avoid obstacles in the local space with a low computational cost.

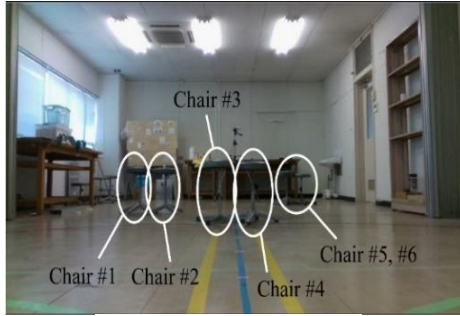
Meanwhile, learning-based methods have been focused on solving the problem of collision avoidance under more dynamic and complicated situations, such as multiple robots or human coexisting environments. In these studies, reinforcement learning or inverse reinforcement learning, popular machine learning methods, have been implemented [11,12,13,14]. The behaviors of the robot were obtained by repetitive training of the network with many frames of avoidance data. Although a higher computational cost is required, a high possibility for the robot to avoid a collision is expected, even if the obstacle moves irregularly.

Although learning-based path planning is attractive, we adopt a simpler method using depth information only because the aim is to verify the effectiveness of physical interaction-based navigation at this time. The system builds a collision-free area map using the depth image obtained by RealSense D435i and guides the user to a secure route with steered wheels. RealSense D435i provides both RGB and depth images, as illustrated in

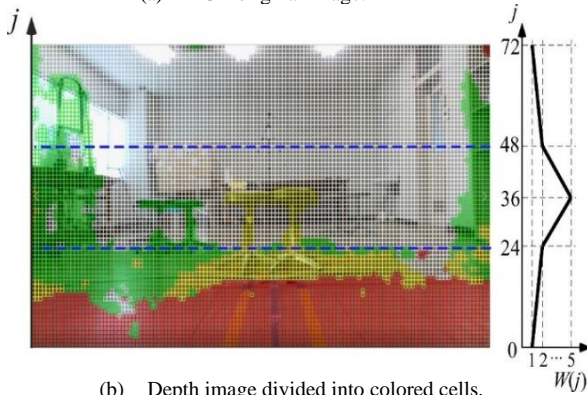
Fig.7(a) and (b). As shown in Fig.7(a), four chairs are present in front of the user.

First, this image area is divided into 9216 (128×72) cells, with a size of 10×10 pixels, as shown in Fig.7(b). The smallest depth value in each cell is defined as its representative depth value, d_{min} .

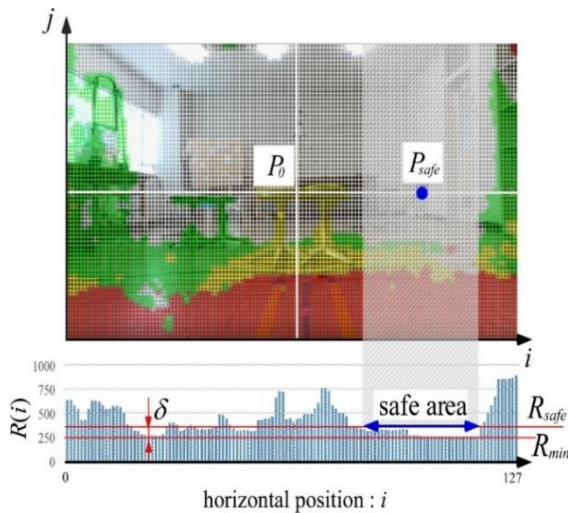
Second, we ranked all cells based on the representative depth value and expressed the result as a four-colored region image. Accordingly, the red, yellow, and green areas cover depths ranging from 0 – 2.0 m, 2.0 – 3.0 m, and 3.0 – 4.0 m, respectively.



(a) RGB original image.



(b) Depth image divided into colored cells.



(c) Safety histogram.

Figure 7. Example of RGB image and colored cell image according to depth value.

It should be noted that the region beyond 4.0 m remains unchanged. We evaluated each direction with respect to

the possibility of secure walking; therefore, all cells were given three kinds of risk levels, $r(i, j)$, according to their colors, namely depth values, $d_{min}(i, j)$ where i and j denote the horizontal and vertical positions of each cell in the image, respectively ($i = 1 - 128$ and $j = 1 - 72$). The risk levels are as follows:

$$r(i, j) = \begin{cases} 10 & \text{for } 0.0 < d_{min}(i, j) \leq 2.0\text{m} \\ 7 & \text{for } 2.0 < d_{min}(i, j) \leq 3.0\text{m} \\ 4 & \text{for } 3.0 < d_{min}(i, j) \leq 4.0\text{m} \\ 0 & \text{for } 4.0\text{m} < d_{min}(i, j) \end{cases} \quad (10)$$

Subsequently, we focused on detecting obstacles more than 2.0 m ahead to allow avoidance. As shown in Fig.7(b), the walking space of the user, which is further than 2.0 m ahead, occupies the horizontal band across the middle of the image. Therefore, the risk level in that region was emphasized by applying the weighting filter, $W(j)$; which consists of four linear functions, defined by the height position as follows:

$$W(j) = \begin{cases} \left(\frac{j}{24}\right) + 1 & \text{for } 0 < j < 24 \\ \left(\frac{j}{4}\right) - 4 & \text{for } 24 \leq j < 36 \\ \left(\frac{-j}{4}\right) + 14 & \text{for } 36 \leq j < 48 \\ \left(\frac{-j}{24}\right) + 4 & \text{for } 48 \leq j < 72 \end{cases} \quad (11)$$

Fig. 7(b) illustrates the relationship between the weighting filter, $W(j)$, and height position j .

Ultimately, the risk level of each cell, $r^*(i, j)$, redefined as the product of $r(i, j)$ and $W(j)$ and the risk level for each direction $R(i)$ is obtained by summing $r^*(i, j)$ along the vertical line, j , at each horizontal position,

$$R(i) = \sum_{j=0}^{71} r^*(i, j) \quad (12)$$

$R(i)$ presented as a histogram in Fig.7(c), where a lower value indicates a safer direction.

C. Navigation for Collision Avoidance

First, the lowest value of the safety histogram, R_{min} , is detected, as shown in Fig.7(c). The safety threshold level, R_{safe} , is defined by adding noise, δ , to R_{min} .

$$R_{safe} = R_{min} + \delta \quad (13)$$

We then successively search for the largest region smaller than the safety level, R_{safe} , and determine a route past its center position, P_{safe} . The coordinate of each point on the image plane can be transformed to that in 3D space via SDK; accordingly, the actual direction angle between the center and target point of the image plane, P_0 and P_{safe} , can be calculated. Simultaneously, it can be confirmed that the safe region has sufficient space for the user to pass through by calculating the width of the safe area in 3D space. Lastly, the steered wheels were adequately controlled based on the direction angle, which was updated each time an obstacle is detected.

Consequently, the user could continue walking without colliding with any obstacles.

If sufficient space does not exist, the steered wheels are controlled to remain stationary. A method for recovering from this situation will be proposed in a future work.

V. VERIFICATION OF PERFORMANCE

A. Guidance with Physical Interaction

We investigated the walking of a user wearing the prototype system to confirm the possibility of guidance via steered wheels. Fig.8 shows the reference trajectories to be guided. The red, green, and black lines describe the ideal trajectories of the outer steered wheel when the desired turning direction, θ_d , is set to 60 deg, 45 deg, and 30 deg, respectively. The angles of the outer and inner steered wheels were controlled based on (1), (2), and (3).

Three healthy men in their twenties participated in this experiment. First, they walked blindfolded to 2.0m ahead. Subsequently, the steering angles of the two wheels, θ^r and θ^l , were controlled so that the subject could follow the reference line specified by θ_d .

Fig.9 presents the experimental results, where θ_d was set to 60 deg in the left side. A series of walking scenarios demonstrated that the subject could precisely follow the reference (black) line. Similarly, the subject moved along the reference lines for different values of θ_d .

Here we investigate how the proposed system interacts with the subject and how the direction of walking changes. As explained in (10), we assume that the rotational moment causes the user to change their walking direction. One of the primary elements generating the moment is the resistive forces, $f_{resist}^{r,(l)}$, which can be estimated by producing the change in the rod length and the stiffness of the springs inserted into the rods (see. Fig.2). Therefore, we measured the lengths of the right and left telescopic rods while walking.

Fig.10 and 11 depict the changes in the length of the telescopic rods when turning at 45 deg and 60 deg in the left side, respectively. These results indicate that the rod on the left side began to decrease gradually after the steering control was completed, and finally reached at constant value. The amount of shortening at turning of 45 deg and 60 deg was approximately -5mm and -10mm, respectively. Based on these results, we can infer that a larger moment acted on the subject as the turning angle increased and the walking direction also increased.

Furthermore, we investigate the association between the turning angle and magnitude of the moment in (10). Fig.12 shows the moment calculated from the experimental data for one subject. The white and red circles with red lines indicate the change in moment values according to the turn angle of θ_d on the left and right sides, respectively. The black-dotted line represents the incremental ratio of the theoretically obtained moment, assuming that the user moves ahead with a constant driving force, f .

Theoretical results indicate that the rotational moment decreases when the turning angle exceeds approximately

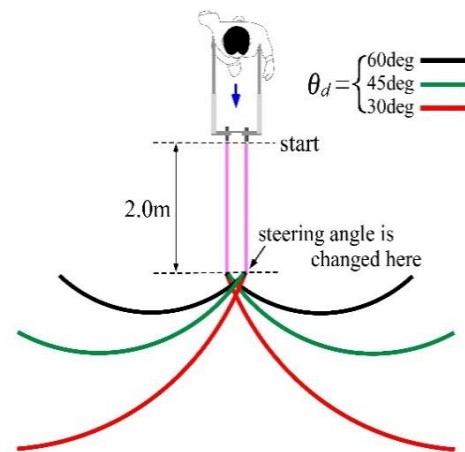


Figure 8. Experiment to evaluate the performance of navigation by steered wheels.

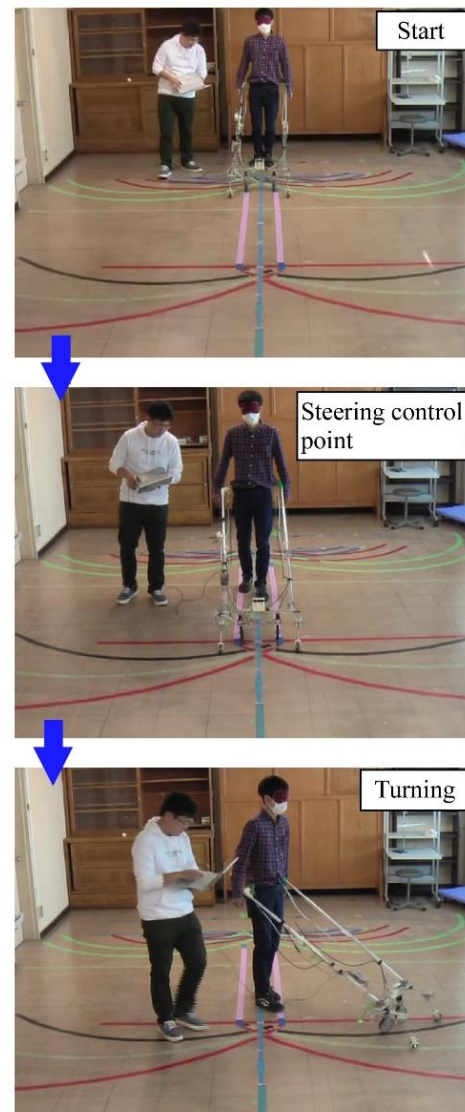


Figure 9. Series of walking scenes guided by steered wheels ($\theta_d = 60deg.$).

60 deg, because the difference between the resistive forces on both sides starts to decrease. Additionally, the steered wheels controlled to be excessive steered angles begin to work as the brake and no longer play the role of a travel aid system. This result indicates the limitation of navigation using the proposed system.

However, the actual moment increased almost proportionally to the magnitude of the turn angle within 60 deg. This indicates that the trend matches the theoretical analysis and the rotational moment acts on the user with sufficient magnitude and helps the user unconsciously change direction.

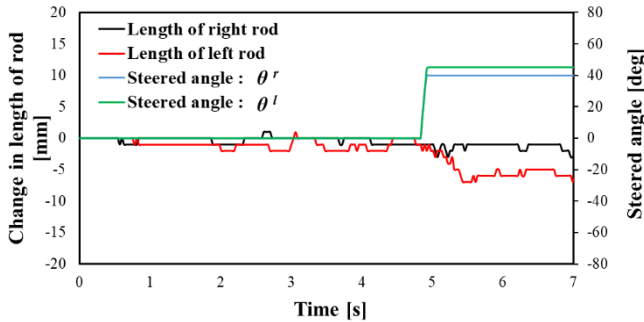


Figure 10. Changes in the length of the telescopic rods (left turn, $\theta_d=45\text{deg.}$).

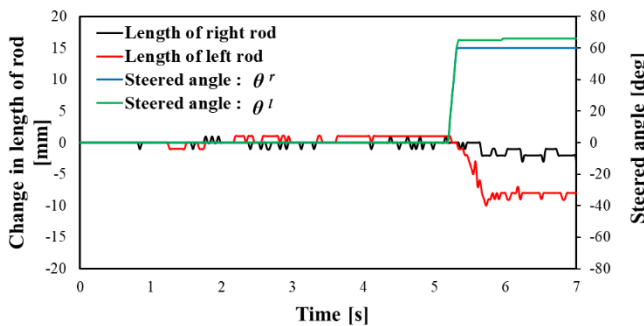


Figure 11. Changes in the length of the telescopic rods (left turn, $\theta_d=60\text{deg.}$).

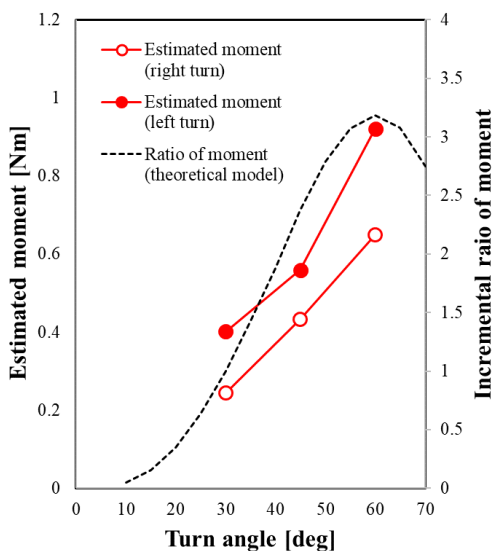


Figure 12. Comparison of the rate of increase of moments obtained experimentally and theoretically.

B. Dent Detection and Fall Prevention

Several experiments were performed to verify the capability of safely stopping the user in terms of the walking speed and steering control time. In this experiment, steering control began when the tilt angle of the stick with the dent detection wheels changed by more than 20 deg. This change is equivalent to a 12 mm change in the height position of the wheels. The steered wheels were placed 166 mm behind the dent detection wheels and the required time allowance for steering control was 0.16 s; therefore, the walking speed should be limited to less than 1.0 m/s.

Three healthy male subjects in their twenties participated in this experiment. Each participant wore a blindfold and attempted the experiment twice without any instructions on walking speed. During each trial, the supporter accompanied the subjects to prevent them from falling when the steering control was delayed or did not work effectively. In such a scenario, all subjects walked carefully; therefore, the walking speed was slower than 1.0 m/s.

Fig.13 illustrates a successful example; the subject approached the step with a velocity of 0.84 m/s and could stop safely via the braking force generated by the steering wheels; that is, the subject succeeded, despite this being the first attempt. Fig.14 depicts the relationship between the displacement of the dent detection wheels and steered angles in this successful case. The dent detection wheels stably sense the unevenness of the floor. Additionally, the steered wheels were controlled successfully to brake the user when the left wheel descended by more than 12mm. The other two subjects could also safely stop before reaching the step.

In the second attempt, two subjects failed despite at mostly consistent walking speed. Consequently, the success rate was 66%.

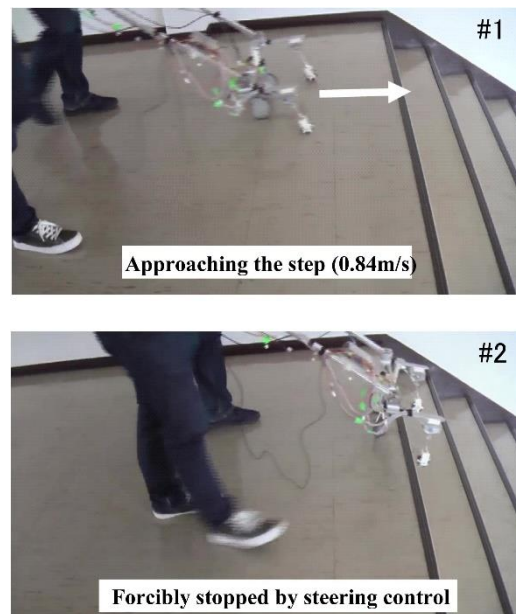


Figure 13. Experiment to verify the capability of emergency stop.

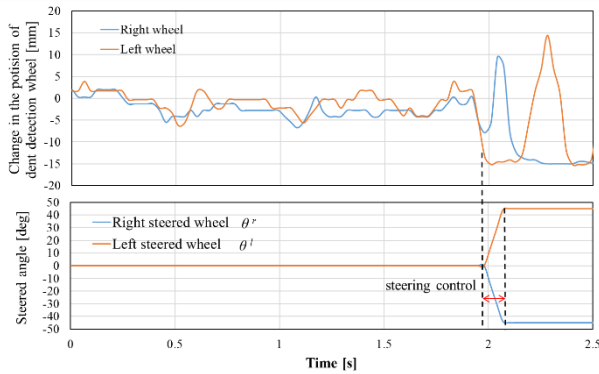


Figure 14. Displacement of the dent detection wheels and the steered wheel angles.

It is inferred that the subjects tended to walk without paying attention, after achieving a good sense of distance to the step from their first attempt. This delays the reaction to the braking wheels. It is well known that the human sensory and musculoskeletal systems have a certain delay when reacting to stimulation. Therefore, we need to account for this delay and devise methods to indicate the step detection earlier to increase safety.

This delayed the reaction of the subject to the brake using by the steered wheels.

C. Collision Avoidance in Actual Environment

We investigated the performance of a guidance system combined with steered wheels and depth camera information. Fig.15 displays a bird's eye view of the test field depicted in Fig.7(a). A healthy male subject, in his twenties, avoided collision with obstacles while walking blindfolded via guidance from the prototype cane system.

In addition, we can suppose that the system guides the subject toward the right side because the free space between Chair#4 and the right wall is wider than that between Chair#3 and Chair#2. Based on this insight, we can predict the optimal path as indicated by the blue arrows passing between Chairs#4 and #5 in Fig.15.

In this experiment, we confirmed that the system could determine the same route and safely guide the subject to track the route. Fig.16 depicts the sequence of images during walking. From these images, it can be confirmed that the subject was guided past the left side of Chair #4, based on the safety histogram shown in Fig.7(c). Subsequently, the system selected the path past the right side of Chair#5 as Chair#6 was too close to the wall; thus, insufficient space was detected on that side. This judgement is the same as our prediction.

The actual path is simplified and described by the dotted red arrows in Fig.15. This path was simply obtained solely from the observation of the subject's walking and shows its tendency and characteristics.

Comparing the predicted and actual paths, it can be noted that the actual path is closer to Chair#5, regardless of the free space between Chairs#5 and #2, because the depth camera cannot sense the entire area between the two chairs because of the limitation of its field of view. However, we can confirm that the subject can go through the obstacle region without colliding with the chairs and

walls by taking advantage of leading the system. The navigation system, comprising steered wheels and a depth camera, performed well for collision avoidance.

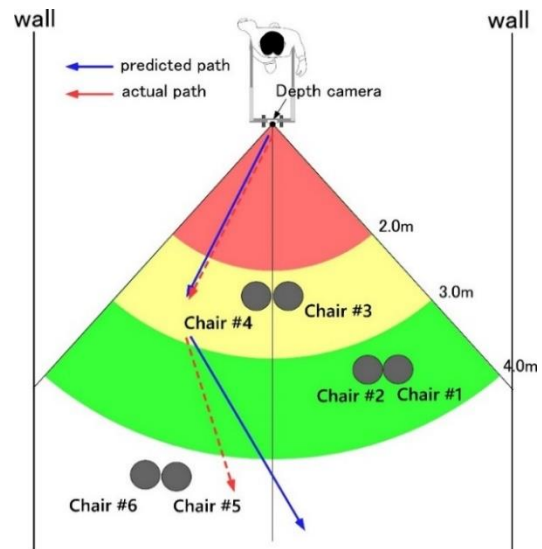


Figure 15. Bird's eye view of test field.

VI. DISCUSSION

Based on the experiments presented in Section V, the depth camera performed well in detecting obstacles and locating safer routes to avoid collisions. Moreover, we confirmed that guiding the user through physical interactions was extremely effective. These functions increase the possibility of the visually impaired moving independently.

However, the response time of the braking mechanism, which is the most crucial function during emergencies, is insufficient. The prototype took approximately 0.16 s from dent detection to complete braking. Furthermore, the reaction time of the user between sensing resistance due to braking and stopping walking should also be considered. Therefore, the allowable walking speed must be limited to approximately 3.0 km/h to prevent dropping off. This value is slower than that of healthy pedestrians, which ranges from 3.2 – 5.5 km/h [15].

This disadvantage can be overcome by locating the dent earlier using the depth camera, which is solely used to detect obstacles in the current prototype. For this purpose, the system should detect the ground and evaluate its discontinuities or degree of unevenness. Several studies have been conducted on this issue [16,17]. In these studies, the flat plane region was extracted using the distance information of each point and is recognized as the ground. Based on these studies, we would like to add ground region detection and unevenness evaluation functions in future developments.

Furthermore, it will be worthwhile incorporating a self-driving ability that uses sensor information from steered

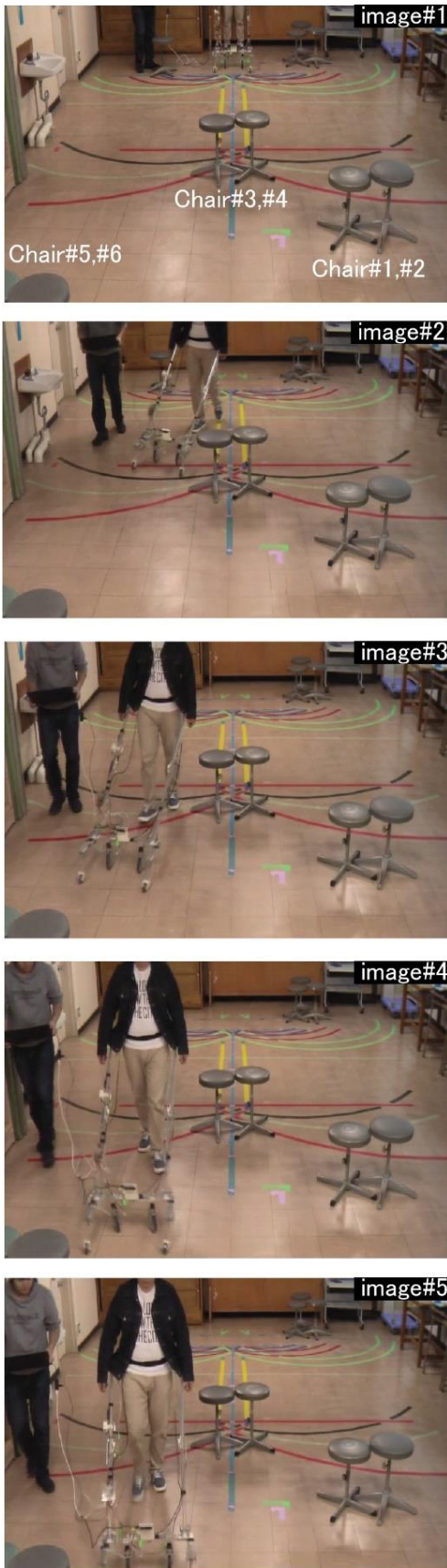


Figure 16. Sequence of images during navigated

wheels and guides the user with respect to speed and direction. Accordingly, smoother and safer guidance can be achieved by considering the walking speed.

VII. CONCLUSION

This study proposes a physical interaction-based walking guidance system. In the proposed system, two passively rotating steered wheels are used to guide the user to a safer route. The steering angles are controlled using information from a depth camera and a dent detection mechanism, which detect obstacles and drop-offs, respectively. The travel resistance of the two wheels is altered by the steering control to act on the waist of the user and to generate a rotational moment. Thus, the user can avoid collisions and continue to walk safely by following this moment. Furthermore, the brake could be immediately applied to the steered wheels when a dent is detected. This function increases the safety.

Previous travel aid systems often provide sound or vibration signals to present obstacles, and the user must distinguish between these changing signals and decide which direction to go in, which places a continuous perceptual and mental burden on the user. The proposed system alleviates the users from this burden and enables them to involuntarily avoid dangerous situations and continue walking safely.

In practical use, it is necessary to improve the response of steering control and its size to facilitate handling.

CONFLICT OF INTEREST

The authors declare no conflict of interest.

AUTHOR CONTRIBUTIONS

Iori WATANABE and Hayato HOSHI designed and fabricated the system and conducted the experiments for evaluating the performance. Shinya KAJIKAWA supervised the research and wrote the paper, all authors had approved the final version.

ACKNOWLEDGMENT

This work was supported by JSPS KAKENHI Grant Number JP19K12901.

REFERENCES

- [1] World Health Organization, Media center, "Vision impairment and blindness, fact sheet (updated October 2017)".
- [2] Y. Wang and K. J. Kuchenbecker, "HALO : Haptic alerts for low hanging obstacles in white cane navigation," in *Proc. of IEEE Haptics Symposium (HAPTICS2012)*, Vancouver, 2012, pp. 527-532.
- [3] S. Gallo, D. Chapuis, L. Santos-Carreras, and Y. Kim et.al., "Augmented white cane with multimodal haptic feedback," in *Proc. of IEEE RAS & EMB International Conference on Biomedical Robotics and Biomechatronics (EMBS2010)*, Tokyo, 2010, pp.149-155.
- [4] R. Pyun, Y. Kim, P. W. Roger, and S. Schneller, "Advanced Augmented white cane with obstacle height and distance feedback," in *Proc. of IEEE international Conference on Rehabilitation Robotics (ICORR2013)*, Seattle, 2013.

- [5] C. Stoll, R. Palluel-Germain, V. Fristot, D. Pellerin, D. Alleysson, and C. Graff, "Navigating from a depth image converted into sound," *Applied Bionics and Biomechanics*, vol. 2015, 543492, 2015.
- [6] Y. H. Lee, and G. G. Medioni, "RGB-D camera based wearable navigation system for the visually impaired," *Computer Vision and Image Understanding*, vol. 149, pp. 3-20, 2016.
- [7] I. Ulrich and J. Borenstein, "The guide cane-applying mobile robot technologies to assist the visually impaired," *IEEE Trans. System, Man, and Cybernetics-Part A: Systems and Humans*, vol. 31, no. 2, pp. 131-136, 2001.
- [8] O. Khatib, "Real-time obstacle avoidance for manipulators and mobile robots," in *Proc. of IEEE International Conference on Robotics and Automation*, 1985, pp. 500-505.
- [9] D. Fox, W. Burgard, and S. Thrun, "The dynamic window approach to collision avoidance," *IEEE Robotics and Automation Magazine*, vol. 4, no. 1, pp. 23-33, 1997.
- [10] J. Borenstein and Y. Koren, "The vector field histogram – fast obstacle avoidance for mobile robots," *IEEE Trans. on Robotics and Automation*, vol. 7, no. 3, pp. 278-288, 1991.
- [11] J. Cao, Y. Wang, and X. Ni, "Multi-robot learning dynamic obstacle avoidance in formation with information directed exploration," *IEEE Trans. on Emerging Topics in Computational Intelligence*, vol. 30, pp. 1-11, 2021.
- [12] Y. Chen, M. Eberett, M. Liu, and J. P. How, "Socially aware motion planning with deep reinforcement learning," in *Proc. of IEEE/RSJ International Conference on Intelligent Robots and Systems (IROS2017)*, 2017.
- [13] H. Kretzschmar, M. Soies, C. Sprunk, and W. Burgard, "Socially compliant mobile robot navigation via inverse reinforcement learning," *The International Journal of Robotics Research*, vol. 35, no. 11, pp. 1289-1307, 2016.
- [14] J. Choi, G. Lee, and C. Lee, "Reinforcement learning-based dynamic obstacle avoidance and integration of path planning," *Intelligent Service Robotics*, vol. 14, pp. 663-677, 2021.
- [15] R. W. Bohannon, A. W. Andrews, and M. W. Thomas, "Walking speed: Reference values and correlates for older adults," *Journal of Orthopaedic & Sports Physical Therapy*, vol. 24, no. 2, pp. 86-90, 1996.
- [16] C. Feng, Y. Taguchi, and V. R. Kamat, "Fast plane extraction in organized point clouds using agglomerative hierarchical clustering," in *Proc. of IEEE International Conference on Robotics and Automation*, Hong Kong, 2014, pp. 6218-6225.
- [17] Z. Jin, T. Tillo, W. Zou, X. Li, and E. G. Lim, "Depth image-based detection," *Big Data Analysis*, vol. 3, no. 1, 2018.

Copyright © 2022 by the authors. This is an open access article distributed under the Creative Commons Attribution License (CC BY-NC-ND 4.0), which permits use, distribution and reproduction in any medium, provided that the article is properly cited, the use is non-commercial and no modifications or adaptations are made.

Shinya Kajikawa received the B.E., M.E, and Ph.D. degrees in mechanical engineering from Tohoku University, Sendai, Japan, in 1991, 1993, and 1996, respectively. From 1996 to 2001, he was a Research Associate in the Department of Mechanical Engineering, Miyagi National College of Technology, Miyagi, Japan. From 2001 to 2004, he was an Associate Professor in the Department of Intelligent Machine and Systems, Akita Prefectural University, Akita, Japan. Since 2004, he has been with Tohoku Gakuin University, Tagajo, Japan, where he is currently a Professor in the Department of Mechanical Engineering and Intelligent Systems. From September 2011 to August 2012, he was a visiting professor at Robotics and Embedded systems lab, Technische Universität München. His current research interests include human-centered robotic design, human-robot interaction, and human-machine interface. Dr. Kajikawa is a member of IEEE, the Japan Society of Mechanical Engineers, the Robotics Society of Japan, and the Society of Instrument and Control Engineers.

Iori Watanabe received the M.E. degree in mechanical engineering from Tohoku Gakuin University, Tagajo, Japan, in 2020. His research interests include the design of mechatronics system for human care. He is currently working at Honda Motor Co., Ltd.. Mr. Watanabe is a member of the Japan Society of Mechanical Engineers.

Hayato Hoshi received the B.E. degree in mechanical engineering from Tohoku Gakuin University, Tagajo, Japan, in 2020. His research interests include software development for intelligent robotic systems. He is currently working at TKC Corporation.